Fabrication of High Energy Flexible All-Solid-State Supercapacitor Using Pseudocapacitive 2D-$Ti_3C_2T_x$-MXene and Battery-Type Reduced Graphene Oxide/Nickel-Cobalt Bimetal Oxide Electrode Materials

Amar M. Patil[a], Nutthaphak Kitiphatpiboon[b], Xiaowei An[b], Xiaoqiong Hao[a,c], Shasha Li[d], Xiaogang Hao[c], Abuliti Abudula[b], Guoqing Guan [a,b*]

[a]Energy Conversion Engineering Laboratory, Institute of Regional Innovation (IRI), Hirosaki University, 2-1-3 Matsubara, Aomori 030-0813, Japan

[b]Graduate School of Science and Technology, Hirosaki University, 3 Bunkyo-cho, Hirosaki, Aomori 036-8560, Japan

[c] Department of Chemical Engineering, Taiyuan University of Technology, Taiyuan 030024, P.R. China.

[d]College of Chemical and Biological Engineering, Taiyuan University of Science and Technology, Taiyuan 030012, China

[*] **Corresponding author.**

Tel.: +81-17-762-7756, fax: +81-17-735-5411.

E-mails: guan@hirosaki-u.ac.jp (G. Guan),

Experimental

Preparation of $Ti_3C_2T_X$/ACF electrode

The Ti_3AlC_2-MAX was purchased from FORSMAN, China and used to prepare $Ti_3C_2T_x$ (MXene). Other chemicals were purchased from Wako Chemicals, Japan and used without further purification. The carbon fiber substrates were treated with conc. HNO_3 (69-70% mass/mass (1.42 g/ml)) for 24 h and washed with deionized water (DI) water for several times to obtain the acid treated carbon fiber (AFC) substrates (3×3 cm^2), which were used as the current collectors of electrodes. The $Ti_3C_2T_x$ was prepared by etching of Al from Ti_3AlC_2 using minimal intensive layered delamination (MILD) method with an in-situ HF formation process. In a typical process, 0.8 g of LiF was slowly added in 10 ml of 9 M HCl solution with stirring. Then, 0.5 g of Ti_3AlC_2 powder was added slowly into this solution in a period of 10 min with continuous stirring, which was kept at 35 ^oC for 24 h under stirring. Thereafter, it was centrifuged under 3500 rpm for 5 min and washed with DI water for several times until pH became 6~7. Finally, the obtained dark supernatant of $Ti_3C_2T_x$ was drop casted on the ACF support. The coated electrode was dried in vacuum oven at 50 ^oC. The mass loading amounts of 0.9-2 mg/cm^2 of $Ti_3C_2T_x$ on ACF were adjusted by repeating drop-casting and drying process.

Preparation of $NiCo_2O_4$@rGO/ACF electrode

Initially, graphene oxide (GO) was synthesized by using the traditional Hummers method. Then, 0.5 g of GO powder was dispersed in 20 ml of DI water with ultrasonic treatment

for 4 h. Thereafter, the GO-sheets dispersed solution was used to prepare the GO-coated ACF by a dip-dry process. Herein, in order to obtain a uniform coating of GO sheets with a proper mass loading amount, the dip-dry process was repeated for 15 times. In the next step, 0.05 M $Ni(NO_3)_2.6H_2O$, 0.1 M $Co(NO_3)_2.6H_2O$, 0.5 M urea and 0.2 M NH_4F were added in 50 ml of DI water and stirred for 10 min and the obtained solution was transferred into a 100 ml Teflon-lined stainless autoclave. Then, the prepared GO/ACF electrode (3×3 cm^2) was immersed in the solution and the autoclave was heated to 150 ^oC in oven for 5 h. After cooled down, the electrode was collected from the autoclave, rinsed in DI water for several times to remove the remained chemicals and those loosely bounded materials, dried at 50 ^oC in oven for 12 h, and further annealed at 300 ^oC for 3 h. Meanwhile, other two electrodes were also fabricated at 170 and 190 ^oC, respectively, with the same precursor solution. The mass loading of $NiCo_2O_4$@rGO electrode material (synthesized at 170 ^oC) on AFC was 1.12 mg/cm^2.

Fabrication of flexible all-solid-state hybrid supercapacitor (FHSCS)

Initially, the PVA-KOH electrolyte was prepared by dissolving 6 g of polyvinyl alcohol (PVA) in 60 ml of DI water and heated at 70 □C with continuous stirring until the solution became transparent state. After that, the 20 ml of 6 M KOH solution was slowly added in the above PVA solution and stirred for 2 h to obtain a gel-like solution of PVA-KOH, which was poured in a porcelain plate and placed at room temperature for 24 h. As such, a flexible and stretchable thin solid PVA-KOH electrolyte film was formed. Herein, the thickness of thin

solid electrolyte film was adjusted by changing the amount of gel-like solution. Finally, the FHSC device was fabricated by sandwiching $NiCo_2O_4$@rGO/ACF positive and $Ti_3C_2T_x$/ACF negative electrodes with the solid PVA-KOH electrolyte film. The size of the FHSC device was 2×1 cm^2 with a footprint area of 2 cm^2 and a volume of 0.133 cm^3 (2×1×0.0668 cm^3).

Characterizations of electrodes

Characterizations of the prepared electrodes and the powder samples were carried out by using different techniques. The structural properties and material confirmation were carried out by using an X-ray diffraction (XRD) spectroscopy equipped with a Cu K_α radiation source (λ= 1.5406 Å) (Rigaku Smart Lab). The surface morphology was observed by a scanning electron microscopy (SEM) (Hitachi SU6600, Japan) and the nanostructure was determined by a transmission electron microscopy (TEM) (JEOL, JEM-2100F). Elemental distributions were determined using an energy-dispersive X-ray spectrometry (EDS) (Horiba EMAX) and the chemical compositions and valences were measured by an X-ray photoelectron spectroscopy (XPS) (VG Scientific ESCALab250i-XLunit, UK). The UV-vis spectra of materials were recorded using UV-vis spectrophotometer V-650 JASCO. The mass of electroactive materials was determined by a Sensitive weight balance SHIMADZU AUW220D.

Electrochemical measurements

All three-electrode and two-electrode electrochemical measurements were measured on a Solartron SI1280B and PAR Versa STAT 4 systems. The three-electrode

electrochemical measurements of both $NiCo_2O_4$@rGO/AFC and $Ti_3C_2T_X$/AFC electrodes were tested in 3M KOH electrolyte. The platinum wire, Hg/HgO electrode and synthesized electrodes were used as counter, reference and working electrodes, respectively. The electrochemical properties of $NiCo_2O_4$@rGO/AFC electrode were tested within a potential range from -0.2 to 0.6 V/vs Hg/HgO. For the negative electrode, the potential range was from -1.0 to -0.2 V/Hg/HgO. For the testing of FHSC, two-electrode system was used. The counter and reference electrodes had connected each other. The ionic diffusion coefficients of both electrodes were calculated based on the CV analysis. The relationship was based on the Randles–Sevcik equation as below.

$$i_p = 2.69 \times 10^5 n^{3/2} A D^{1/2} C_0 v^{1/2} \quad \text{(S1)}$$

$$D = \left[\frac{B\ (Slope)}{2.69\times10^5\ \times n^{3/2}\ AC_0}\right]^2 \quad \text{(S2)}$$

i_p = current maximum in amps

n = number of electrons transferred in the redox event (usually 1)

A = electrode area in cm^2

D = diffusion coefficient in cm^2/s

C = concentration in mol/cm^3

v = scan rate in V/s

The specific and areal capacitances of electrodes and the FHSC device were determined by integrating the discharge portion of CV curve using the following equations.

$$\text{Specific Capacitance } = \frac{1}{\text{Vmv}} \int \text{idV} \quad \text{(S3)}$$

Areal Capacitance $= \frac{1}{VA\nu} \int i dV$ (S4)

where, 'm' is mass of loaded electrode material in mg, 'ν' is the scan rate in mV/s, 'V' is operating potential window, 'i' is current in mA and A is footprint area of electrode surface. The total mass loading of asymmetric supercapacitor was calculated by considering masses of positive and negative electrode materials. For the FHSC device, since the positive and negative electrodes were sandwiched with the PVA-KOH solid electrolyte, the geometrical footprint area of one electrode was considered. From GCD analysis, the specific, areal and volumetric capacitances of electrodes and the FHSC device were calculated by integrating discharge portion using following equations,

Specific Capacitance

$$= \frac{I \times \int V dt}{M \times V^2}$$

Areal Capacitance

$$= \frac{I \times \int V dt}{Area \times V^2}$$

Volumetric Capacitance

$$= \frac{I \times \int V dt}{Volume \times V^2}$$ (S

Specific, areal and volumetric energy densities and power densities of the FHSC device were calculated by using following equations,

Specific energy density $= \frac{1}{2 \times 3600} C_s V^2$ and

(S8)

Specific power density

$$= \frac{ED \times 3600}{T_d}$$

Areal energy density $= \frac{1}{2 \times 3600} C_A V^2$ and

(S10)

Areal power density $=$

$$\frac{ED_A \times 3600}{T_d}$$

Volummetric energy density $= \frac{1}{2 \times 3600} C_V V^2$ and

(S12)

Volumetric power density $=$

$$\frac{ED_V \times 3600}{T_d} \quad \text{(S13)}$$

where, M is total mass of both electrode materials; C_s, C_A and C_V are specific, areal and volumetric capacitances, respectively; ED, ED_A, ED_V are specific, areal and volumetric energy densities, respectively; 'T_d' is discharging time, V is potential window.

The mass loading amounts on both electrodes were adjusted using following equation,

$$\frac{M^+}{M^-} = \frac{C_s^- \times V^-}{C_s^+ \times V^+}$$

where, 'M^+' and 'M^-' are masses of electroactive materials of $NiCo_2O_4$@rGO and $Ti_3C_2T_X$; 'C_s^+' and 'V^+' are C_s and potential window of the $NiCo_2O_4$@rGO/ACF

electrode, respectively; 'C_s^-' and 'V^-' are C_s and potential window of the $Ti_3C_2T_X$/ACF electrode, respectively.

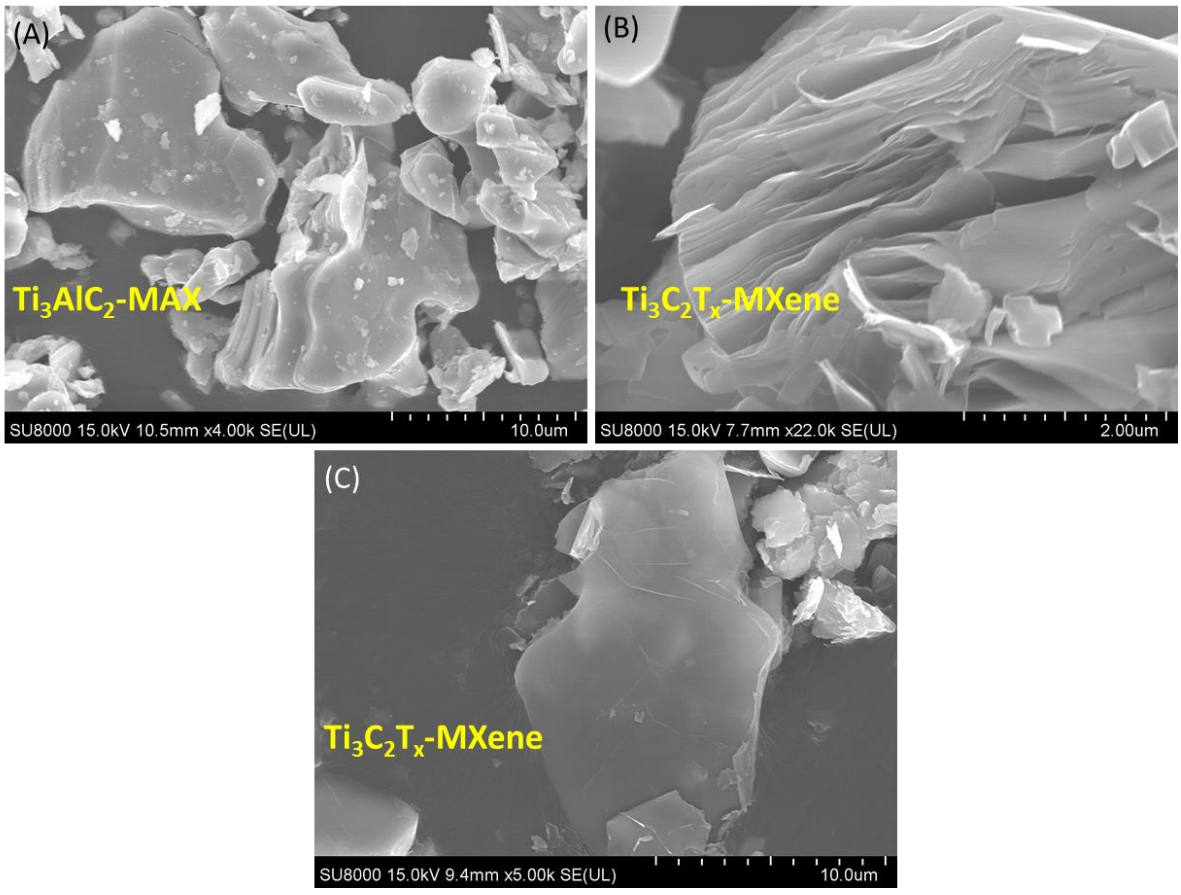

Figure S1 SEM images of (A) Ti_3AlC_2-MAX, (B) delaminated $Ti_3C_2T_x$-MXene, and (C) exfoliated $Ti_3C_2T_x$.

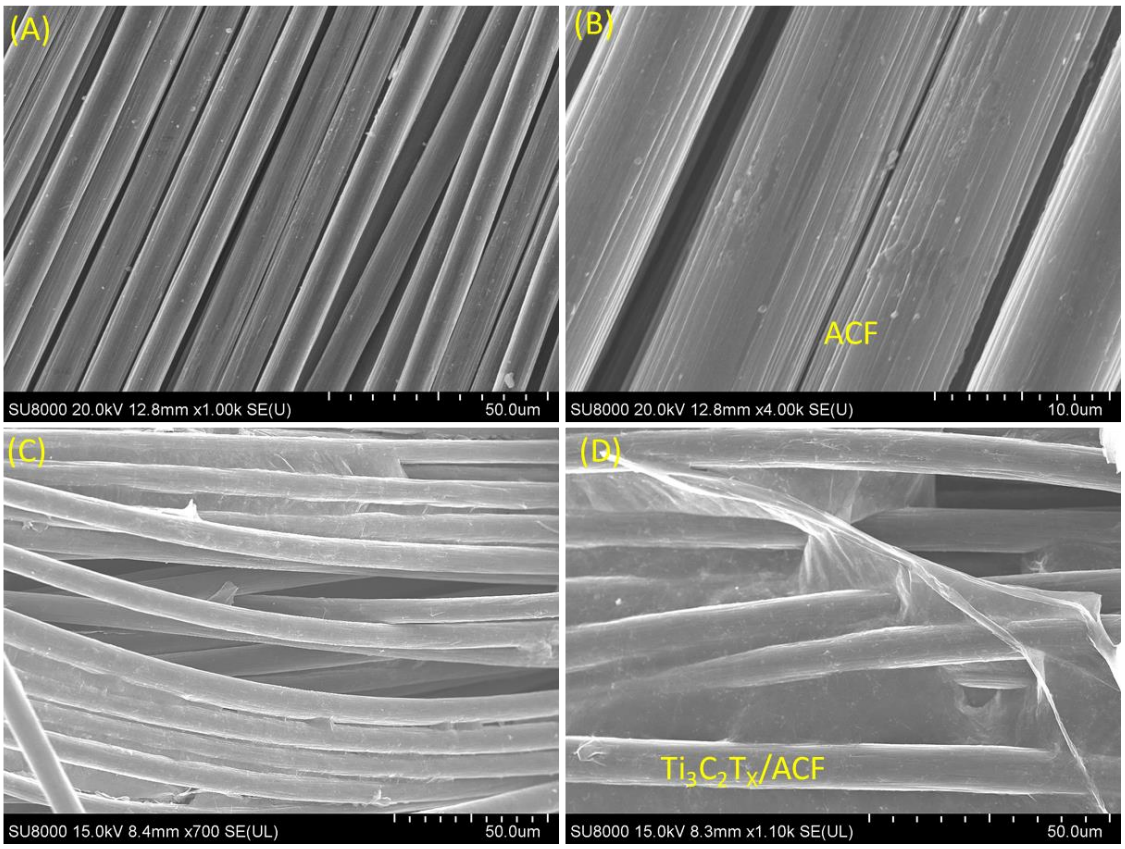

Figure S2 (A and B) SEM images of acid treated carbon fiber (ACF), and (C and D) SEM images of $Ti_3C_2T_x$/ACF electrodes.

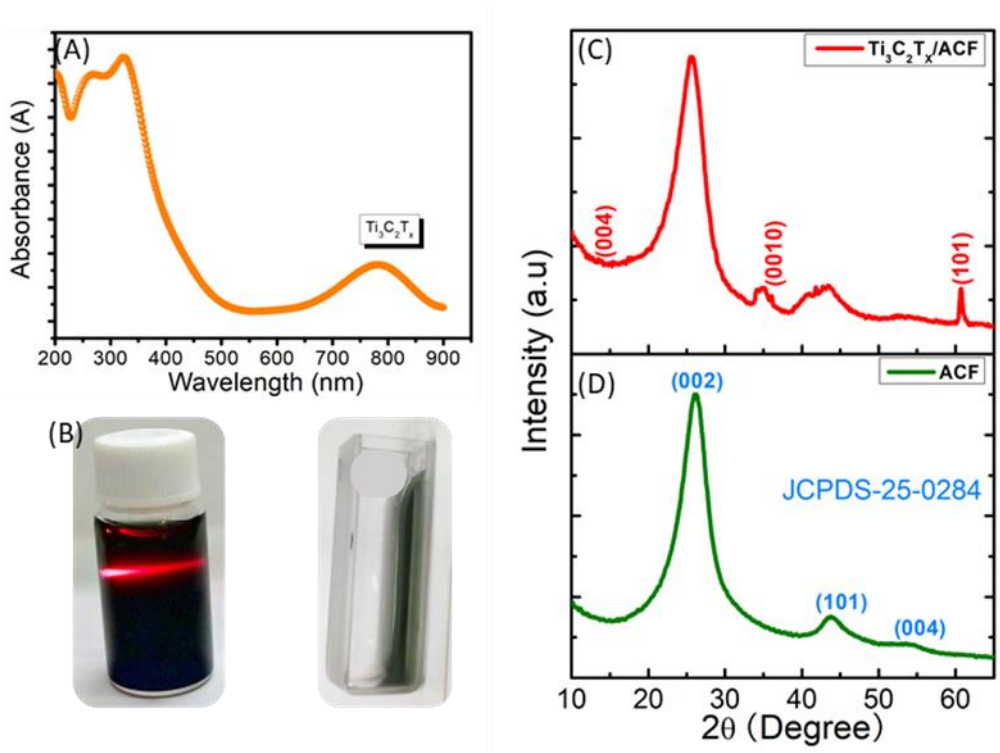

Figure S3 (A) Absorbance versus wavenumber plot for diluted $Ti_3C_2T_x$-MXene ink, (B) photographs of the prepared $Ti_3C_2T_x$-MXene ink and the Tyndall effect of it, (C and D) XRD patterns of $Ti_3C_2T_x$/ACF and ACF.

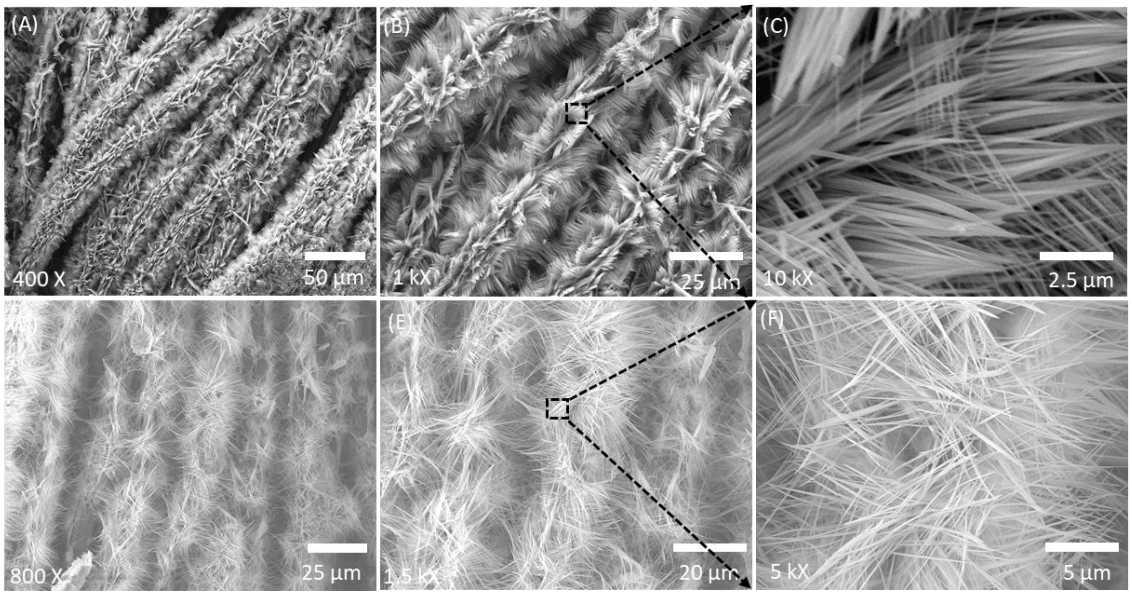

Figure S4 SEM images of $NiCo_2O_4$@rGO/AFC electrode deposited at (A-C) 150 and (D-F) 190 °C

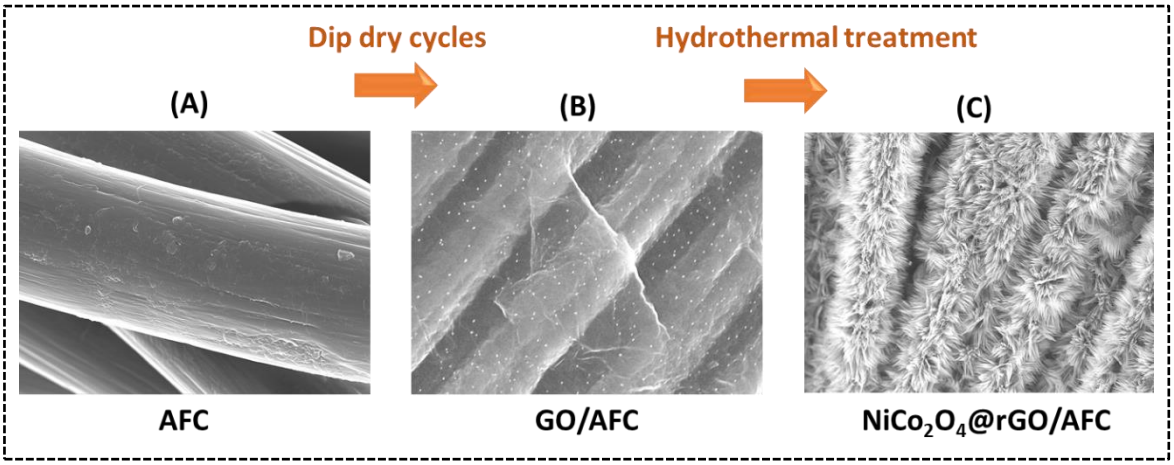

Figure S5 SEM images of (A) HNO_3 treated carbon fiber (ACF), (B) GO/ACF, and (C) $NiCo_2O_4$@rGO/ACF.

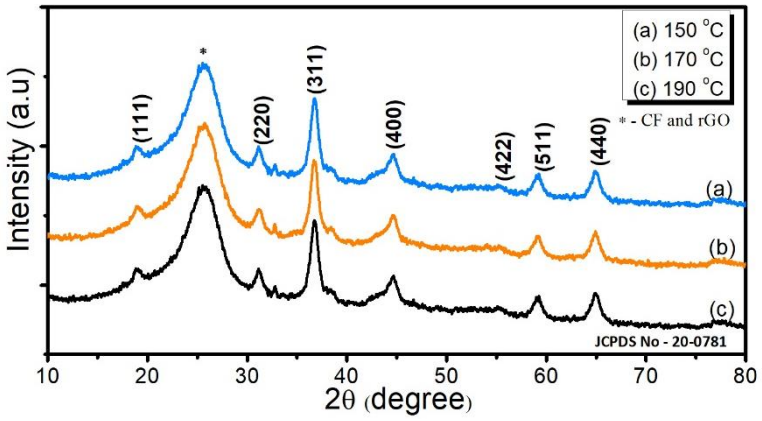

Figure S6 XRD patterns of $NiCo_2O_4$@rGO/AFC electrodes deposited at 150, 170 and 190 °C.

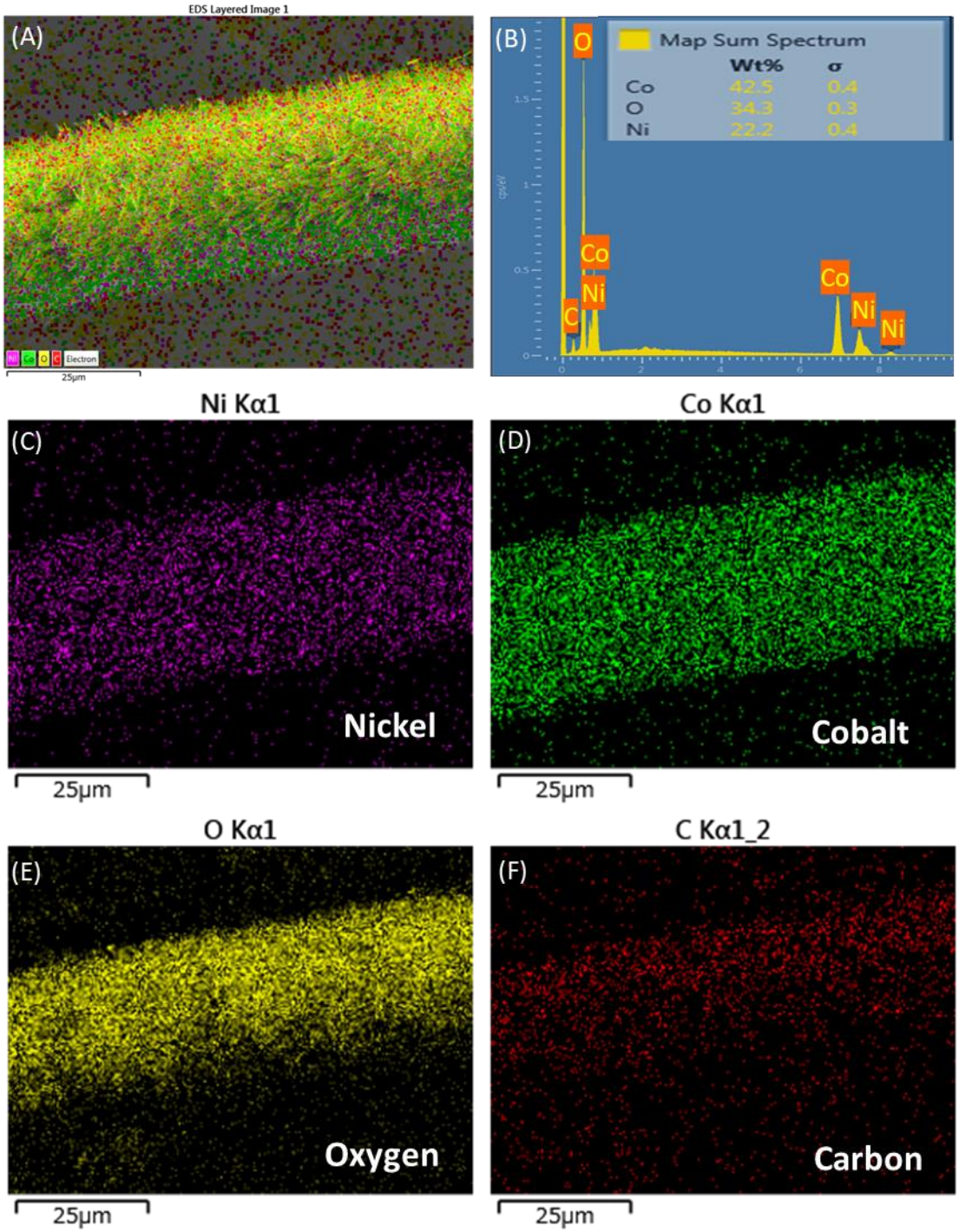

Figure S7 (A) SEM for elemental mapping of $NiCo_2O_4$@rGO/ACF, (B) EDS spectrum, and elemental mappings of (C) Nickel (Ni), (D) Cobalt (Co), (E) Oxygen (O) and (F) Carbon (C) elements.

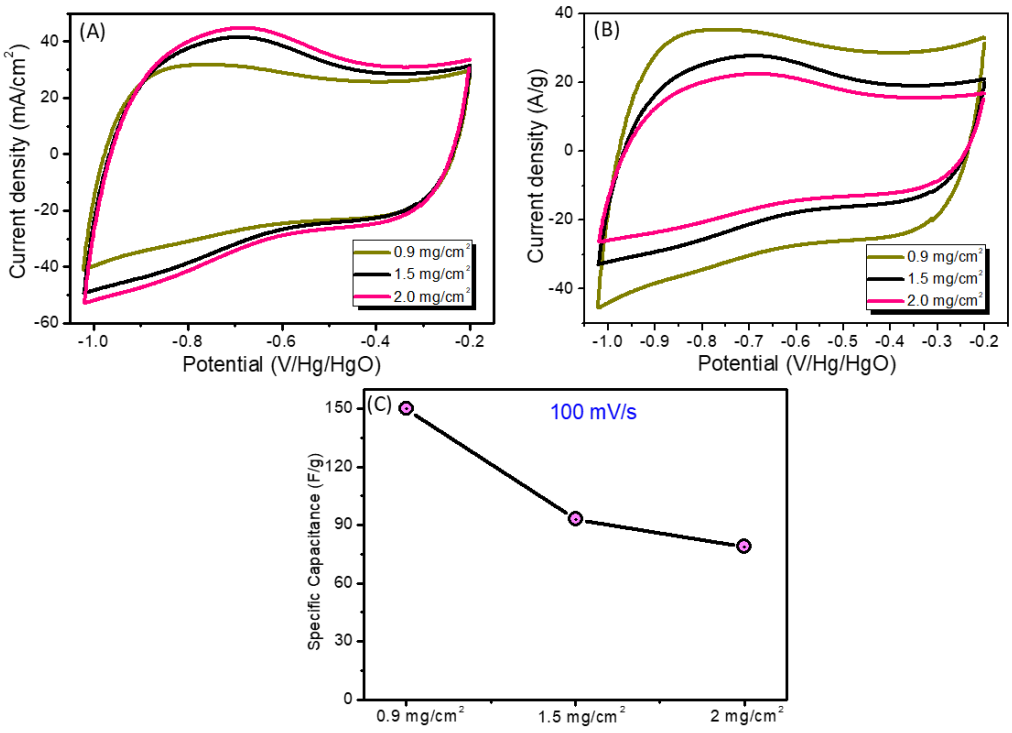

Figure S8 (A and B) CV curves of $Ti_3C_2T_X$/AFC electrode measured at a scan rate of 100 mV/s with the loading mass amounts of 0.9, 1.5 and 2 mg/cm^2 considering per unit area (cm^2) and mass (g), and (C) specific capacitance of all three electrodes.

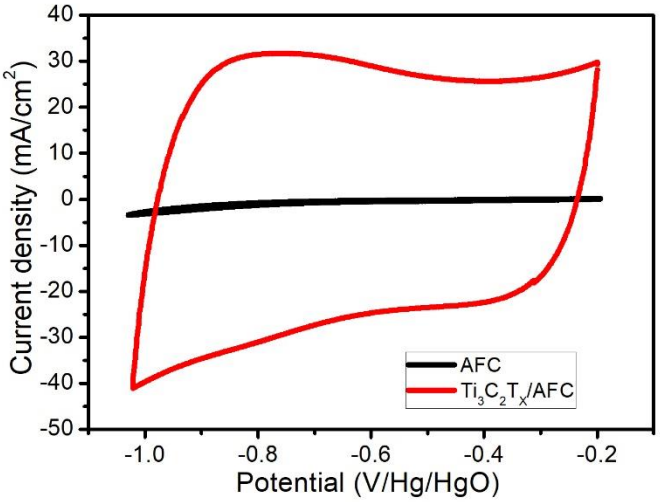

Figure S9 CV curves of AFC and $Ti_3C_2T_X$/AFC electrodes.

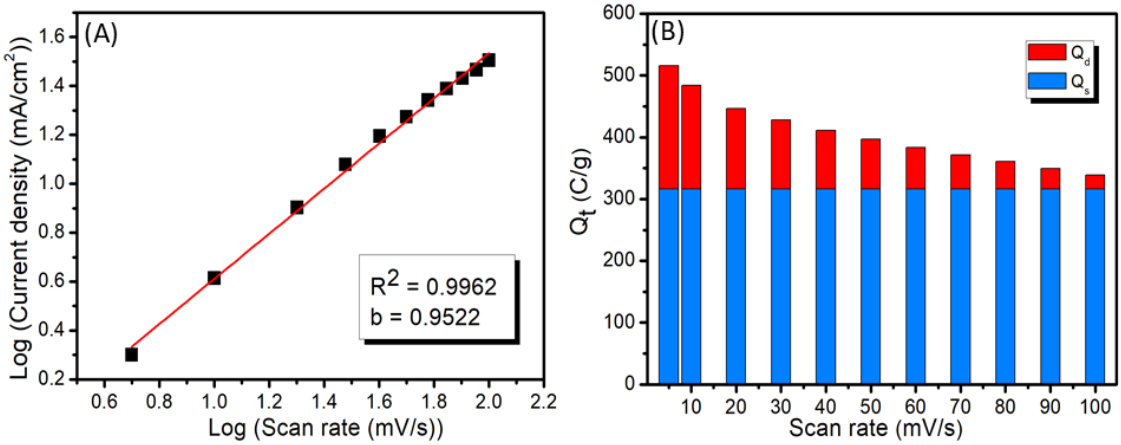

Figure S10 (A) Plot of log of current density versus log of scan rate, and (B) Total charge stored on the electrode at different scan rates for the $Ti_3C_2T_x$/ACF electrode.

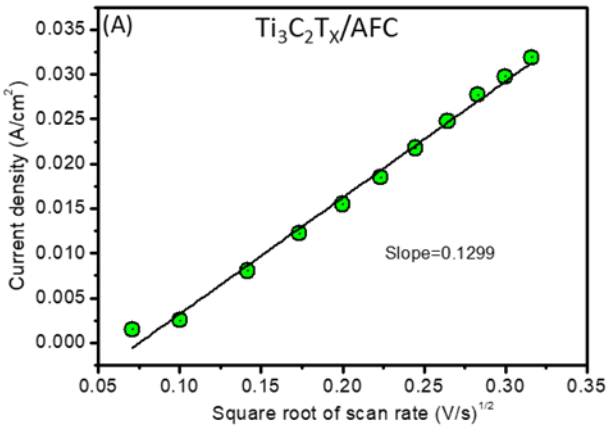

Figure S11 Current density versus square root of scan rate plot of $Ti_3C_2T_X$/AFC electrode.

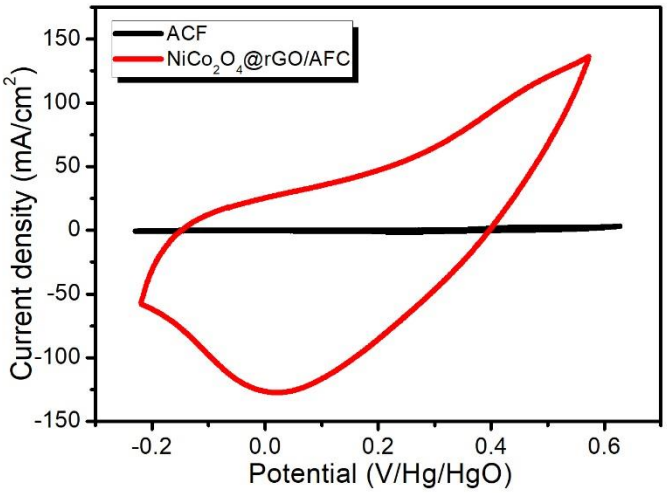

Figure S12 CV curves of AFC and $NiCo_2O_4$@rGO/ACF electrodes at a 100 mV/s scan rate.

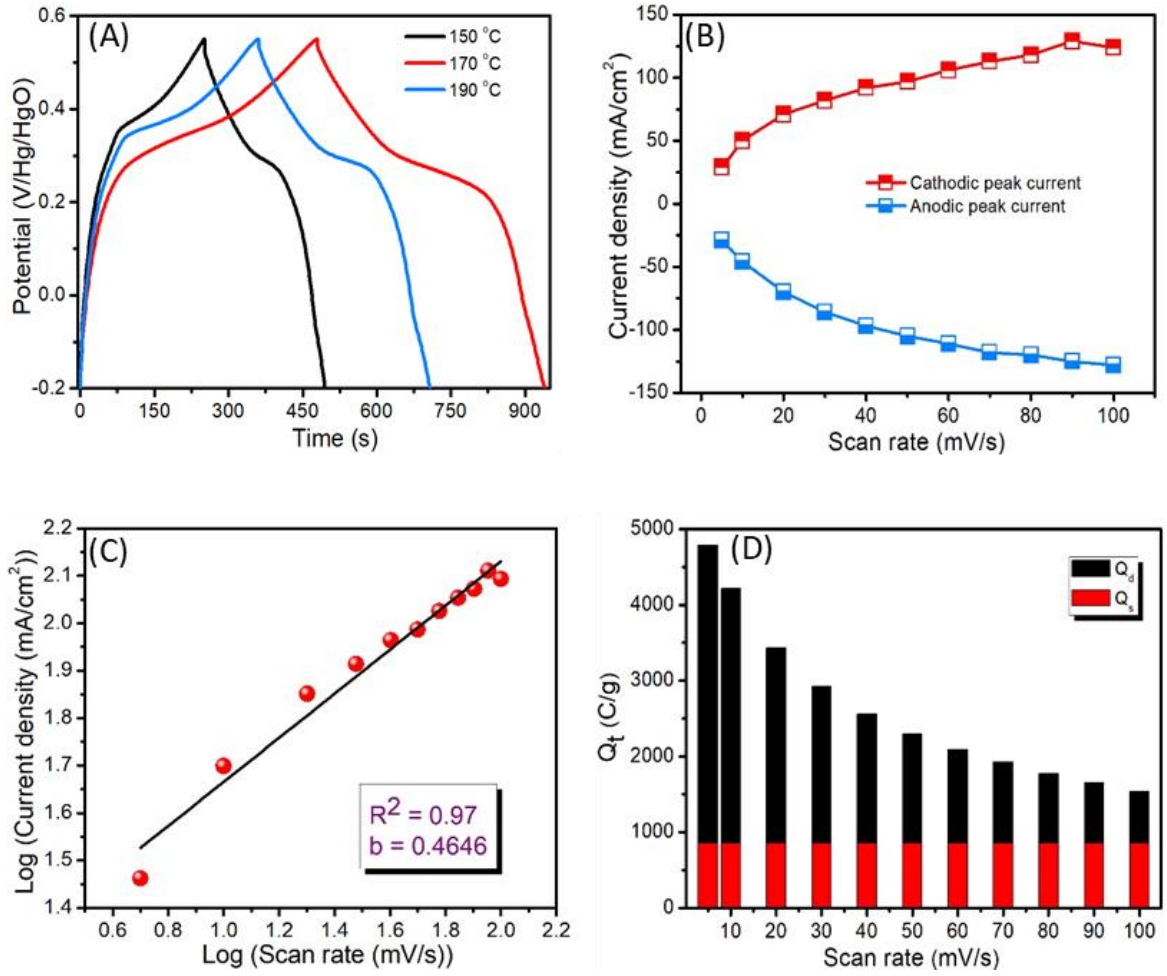

Figure S13 (A) GCD curves of $NiCo_2O_4$@rGO/ACF electrodes prepared at the hydrothermal synthesis temperatures of 150, 170 and 190 °C, (B) current density versus scan rate plots, (C) log of current density versus log of scan rate plot, which gives R^2 and b values, and (D) total charges stored on the $NiCo_2O_4$@rGO/ACF electrode at different scan rates.

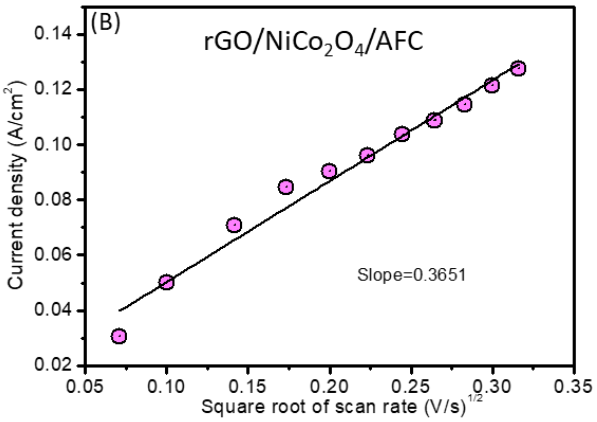

Figure S14 Current density versus square root of scan rate plot of $NiCo_2O_4$@rGO/ACF electrode.

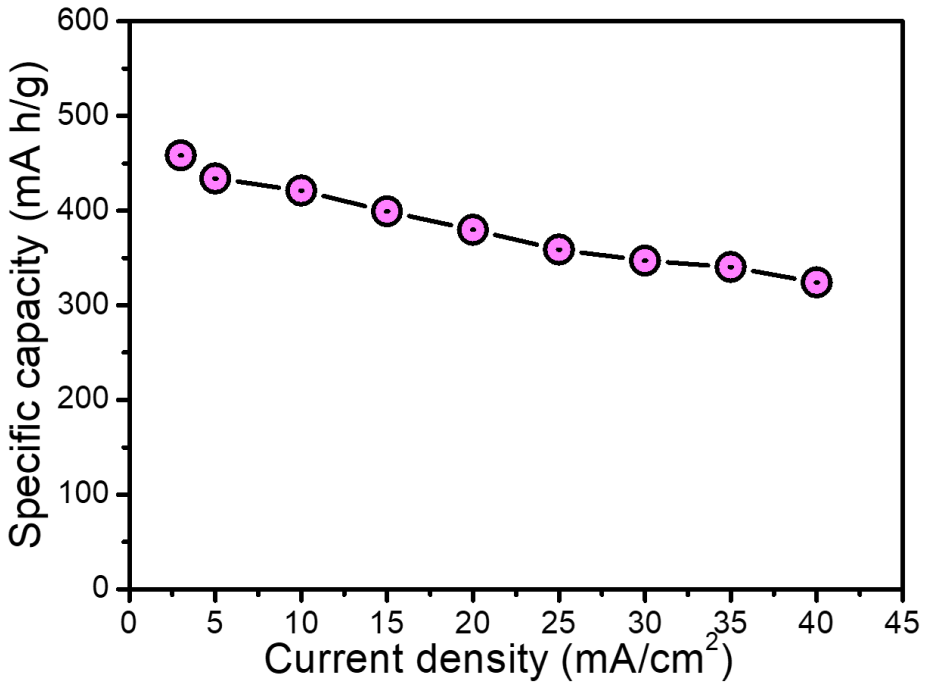

Figure S15 Specific capacity versus current density plot of $NiCo_2O_4$@rGO/AFC electrode.

Figure S16 Photographs of thickness measurement of the negative electrode.

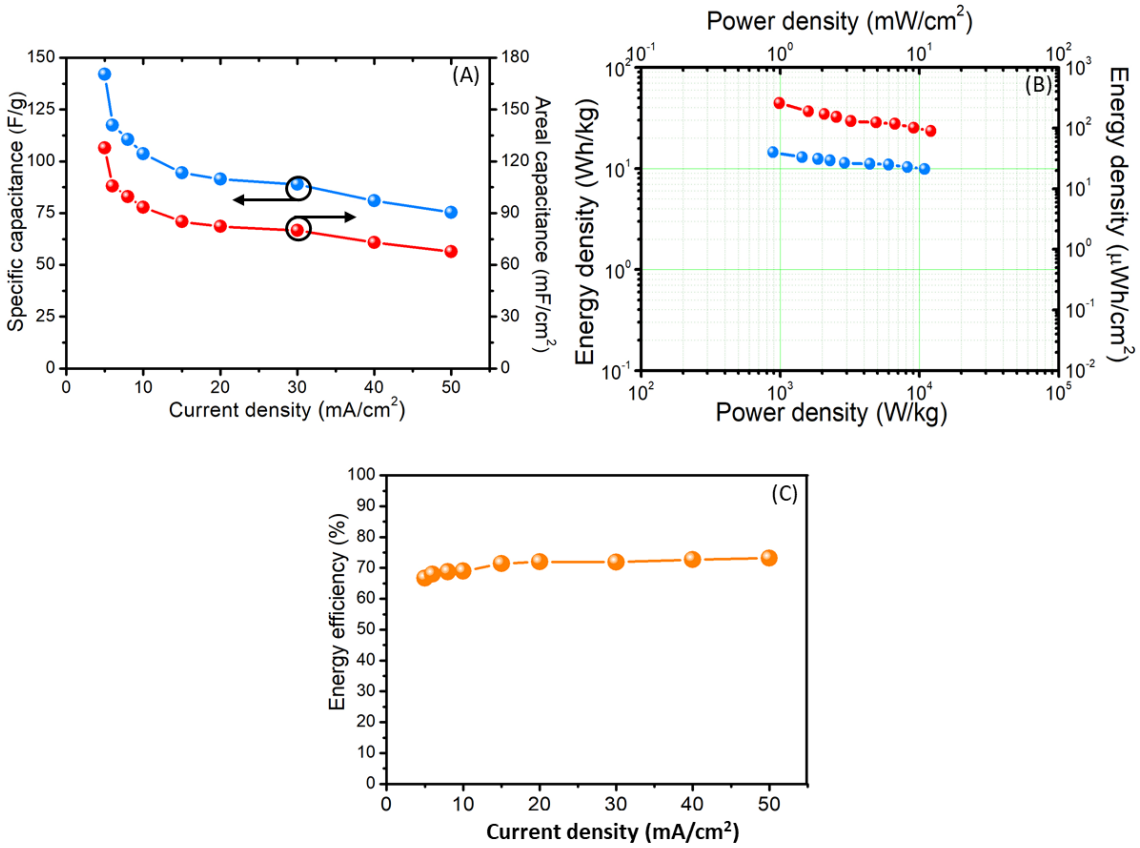

Figure S17 (A) Specific and areal capacitances versus current density plots, (B) Ragone plot and (C) Energy efficiency versus current density plots of the FHSC device.

Table S1 Electrochemical performances of various $Ti_3C_2T_X$ based electrodes.

Electrode Material	Electrolyte	Capacitance	Stability (%)	Potential (V)	Ref
N□doped $Ti_3C_2T_x$	6 M KOH	156–122 F/g (5–200 mV/s)	100 (5000 cycles)	−1 – − 0.4	1
N□doped $Ti_3C_2T_x$	6 M KOH	266–210 F/g (5–200 mV/s)	86.4 (2000 cycles)	−1 – −0.4	2
$Ti_3C_2T_x/MoO_3$	1 M KOH	151–105 F/g (2–100 mV/s)	93.7 (8000 cycles)	−1 – −0.3	3
$Ti_3C_2T_x/SnO_2$	6 M KOH	125□100 F/g (1–10 A/g)	82 (8000 cycles)	−1 – −0.3	4
$Ti_3C_2T_x/MnO_2$	6 M KOH	377–317 mF/cm^2 (5–200 mV/s)	95 (5000 cycles)	−1 – −0.4	5
$Ti_3C_2T_x/TiO_2$ NWs	6 M KOH	143–106 F/g (2–100 mV/s)	80 (6000 cycles)	−1 – −0.4	6
$Ti_3C_2T_x$–TiO_2	6 M KOH	143–117 F/g (5–200 mV/s)	92 (6000 cycles)	−1 – −0.35	7
$Ti_3C_2T_x$@PPy	1 M KOH	610□302 F/g (0.5–25 A/g)	100 (14 000 cycles)	0 – 0.6	8
$Ti_3C_2T_x$/PVA	1 M KOH	528–310 F/cm^3 (2–100 mV/s)	≈85 (10 000 cycles)	−1 – −0.4	9
$Ti_3C_2T_x$ □OMC	6 M KOH	198□150 F/cm^3 (1–20 A/g)	-	−1 – −0.4	10
NC□$Ti_3C_2T_x$	6 M KOH	82.8–49.5 F/g (1–100 A/g)	100 (5000 cycles)	−1.05 – − 0.15	11
$Ti_3C_2T_x$/SWCNT	1 M KOH	314–205 F/cm^3 (2–100 mV/s)	95 (10 000 cycles)	−1 – −0.5	12
rGO/$Ti_3C_2T_x$	6 M KOH	370□206 F/cm^3 (0.92–9.2 A/cm^3)	100 (10 000 cycles)	−1 – −0.3	13
$Ti_3C_2T_x$/rGO	2 M KOH	154.3–141.7 F/g (1□5 A/g)	85 (6000 cycles)	−0.7 – 0	14
d□	6 M KOH	393–314 F/cm^3	100 (10 000	0.1 – 0.55	15

$Ti_3C_2T_x$/CNT		(5–100 mV/s)	cycles)		
$Ti_3C_2T_x$ foam	1 M KOH	271□178 mF/cm^2 (5–100 mV/s)	88.7 (10 000 cycles)	−1 – −0.5	16
$Ti_3C_2T_x$ aerogel	1 M KOH	1013–520 mF/cm^2 (2–100 mV/s)	95 (10 000 cycles)	−1 – −0.4	17
$Ti_3C_2T_x$ paper	1 M KOH	295□235 F/cm^3 (2–100 mV/s)	94.4 (15 000 cycles)	−0.9 – −0.4	18
$Ti_3C_2T_x$ film on Ni foam	1 M KOH	246–177 mF/cm^2 (5–50 mV/s)	100 (10 000 cycles)	−0.75 – 0.25	19
$Ti_3C_2T_x$ film	1 M KOH	340 F/cm^3 (2 mV/s)	100 (10 000 cycles)	−0.55 – 0	20
$Ti_3C_2T_X$/ACF	3 M KOH	246.9 F/g (197 mF/cm^2) at 4 mA/cm^2	96.7 (5000)	−1.0 – −0.2	This work

References

1. Tang, Y.; Zhu, J. F.; Wu, W. L.; Yang, C. H.; Lv, W. J.; Wang, F. Synthesis of Nitrogen-Doped Two-Dimensional Ti_3C_2 with Enhanced Electrochemical Performance *J. Electrochem. Soc*. **2017**, *164,* A923–A929.

2. Yang, C. H.; Que, W. X.; Yin, X. T.; Tian, Y. P.; Yang, Y. W.; Que, M. D. Improved Capacitance of Nitrogen-Doped Delaminated Two-Dimensional Titanium Carbide by Urea-Assisted Synthesis *Electrochim. Acta* **2017**, *225,* 416–424.

3. Zhu, J. F.; Lu, X.; Wang, L. Synthesis of a $MoO_3/Ti_3C_2T_x$ Composite with Enhanced Capacitive Performance for Supercapacitors *RSC Adv.* **2016**, *6,* 98506–98513.

4. Zheng, W.; Zhang, P. G.; Tian, W. B.; Wang, Y.; Zhang, Y. M.; Chen, J.; Sun, Z. M. Microwave-Assisted Synthesis of SnO_2-Ti_3C_2 Nanocomposite for Enhanced Supercapacitive Performance *Mater. Lett.* **2017**, *209*, 122–125.

5. Tang, Y.; Zhu, J. F.; Yang, C. H.; Wang, F. Enhanced Supercapacitive Performance of Manganese Oxides Doped Two-Dimensional Titanium Carbide Nanocomposite in Alkaline Electrolyte *J. Alloys Compd*. **2016**, *685*, 194–201.

6. Cao, M. J.; Wang, F.; Wang, L.; Wu, W. L.; Lv, W. J.; Zhu, J. F. Room Temperature Oxidation of Ti_3C_2 MXene for Supercapacitor Electrodes *J. Electrochem. Soc*. **2017**, *164,* A3933–A3942.

7. Zhu, J. F.; Tang, Y.; Yang, C. H.; Wang, F.; Cao, M. J. Composites of TiO_2 Nanoparticles Deposited on Ti_3C_2 MXene Nanosheets with Enhanced Electrochemical Performance *J. Electrochem. Soc*. **2016**,

163, A785–A791.

8. Le, T. A.; Tran, N. Q.; Hong, Y.; Lee, H. Intertwined Titanium Carbide MXene within a 3 D Tangled Polypyrrole Nanowires Matrix for Enhanced Supercapacitor Performances *Chem. Eur. J.* **2019**, *25,* 1037–1043.

9. Ling, Z.; Ren, C. E.; Zhao, M. Q.; Yang, J.; Giammarco, J. M.; Qiu, J. S.; Barsoum, M. W.; Gogotsi, Y. Flexible and Conductive MXene Films and Nanocomposites with High Capacitance *Proc. Natl. Acad. Sci. USA* **2014,** *111*, 16676–16681.

10. Wang, J.; Tang, J.; Ding, B.; Malgras, V.; Chang, Z.; Hao, X. D.; Wang, Y.; Dou, H.; Zhang, X. G.; Yamauchi, Y. Hierarchical Porous Carbons with Layer-By-Layer Motif Architectures from Confined Soft-Template Self-Assembly in Layered Materials *Nat. Commun*. **2017**, 8, 15717–15725.

11. Zhang, C.; Wang, L.; Lei, W.; Wu, Y. T.; Li, C. W.; Khan, M. A.; Ouyang, Y.; Jiao, X. Y.; Ye, H. T.; Mutahir, S.; Hao, Q. L. Achieving Quick Charge/Discharge Rate of 3.0 V s^{-1} by 2D Titanium Carbide (Mxene) *Via* N-Doped Carbon Intercalation *Mater. Lett*. **2019**, *234,* 21–25.

12. Fu, Q. S.; Wang, X. Y.; Zhang, N.; Wen, J.; Li, L.; Gao, H.; Zhang, X. T. Self-Assembled $Ti_3C_2T_x$/SCNT Composite Electrode with Improved Electrochemical Performance for Supercapacitor *J. Colloid Interface Sci.* **2018**, *511*, 128–134.

13. Xu, S. K.; Wei, G. D.; Li, J. Z.; Han, W.; Gogotsi, Y. Flexible MXene–Graphene Electrodes with High Volumetric Capacitance for Integrated Co-Cathode Energy Conversion/Storage Devices *J. Mater. Chem. A* **2017**, *5,* 17442–17451.

14. Zhao, C. J.; Wang, Q.; Zhang, H.; Passerini, S.; Qian, X. Z. Two-Dimensional Titanium Carbide/RGO Composite for High-Performance Supercapacitors *ACS Appl. Mater. Interfaces* **2016**, *8,* 15661–15667.

15. Yan, P. T.; Zhang, R. J.; Jia, J.; Wu, C.; Zhou, A. G.; Xu, J.; Zhang, X. S. Enhanced Supercapacitive Performance of Delaminated Two-Dimensional Titanium Carbide/Carbon Nanotube Composites In Alkaline Electrolyte *J. Power Sources* **2015**, *284*, 38–43.

16. Shi, L.; Lin, S. Y.; Li, L.; Wu, W. Y.; Wu, L. L.; Gao, H.; Zhang, X. T. $Ti_3C_2T_x$-Foam as Free-Standing Electrode for Supercapacitor with Improved Electrochemical Performance *Ceram. Int.* **2018**, *44,* 13901–13907.

17. Li, L.; Zhang, M. Y.; Zhang, X. T.; Zhang, Z. G. New Ti_3C_2 Aerogel as Promising Negative Electrode Materials for Asymmetric Supercapacitors *J. Power Sources* **2017**, *364*, 234–241.

18. Wu, W. Y.; Lin, S. Y.; Chen, T. T.; Li, L.; Pan, Y.; Zhang, M. Y.; Wu, L. L.; Gao, H.; Zhang, X. T. Performance Evaluation of Asymmetric Supercapacitor Based on $Ti_3C_2T_x$-Paper *J. Alloys Compd.* **2017**, *729*, 1165–1171.

19. Xu, S. K.; Wei, G. D.; Li, J. Z.; Ji, Y.; Klyui, N.; Izotov, V.; Han, W. Binder-Free $Ti_3C_2T_x$ MXene electrode Film for Supercapacitor Produced by Electrophoretic Deposition Method *Chem. Eng. J.* **2017**, *317*, 1026–1036.

20. Lukatskaya, M. R.; Mashtalir, O.; Ren, C. E.; Dall'Agnese, Y.; Rozier, P.; Taberna, P. L.; Naguib, M.; Simon, P.; Barsoum, M. W.; Gogotsi, Y. Cation Intercalation and High Volumetric

Capacitance of Two-Dimensional Titanium Carbide *Science* **2013**, *341,* 1502–1505.